Sensing and Bio-Sensing Research 23 (2019) 100261

Contents lists available at ScienceDirect

Sensing and Bio-Sensing Research

journal homepage: www.elsevier.com/locate/sbsr

Ultra selective label free electrochemical detection of cancer prognostic p53-antibody at DNA functionalized graphene

Habibulla Imran[a], Palinci Nagarajan Manikandan[a], Dhamodharan Prabhu[b], Venkataraman Dharuman[a,*], Jeyaraman Jeyakanthan[b], Jong Hoon Hahn[c]

[a] Molecular Electronics Laboratory, Department of Bioelectronics and Biosensors, Alagappa University, Science Campus, India
[b] Department of Bioinformatics, Alagappa University, Science Campus, Karaikudi 630 003, India
[c] Department of Chemistry and BioNanotechnology Center, Pohang University of Science and Technology, San 31, Hyojadong, Pohang 790-784, South Korea

ARTICLE INFO

Keywords:
Electrical exfoliation
Graphene
DNA
p53 antibody
Selective
Label free

ABSTRACT

Detection of p53 antibody, a universal cancer biomarker, essential for the early diagnosis and prevention of cancer mortality. Here, we report label free electrochemical detection of p53 antibody binding with DNA on a graphene prepared by direct electrical exfoliation of pencil graphite in presence of aminoacid (glycine) in aqueous solution for the first time. Role of glycine in preventing graphitization is analysed using Fourier transform infrared spectroscopy, Raman, X-ray diffractommetry, X-ray photoelectron spectroscopy and transmission electron microscopy. Graphene has been decorated with gold nanoparticles prior to the biofunctionalization with DNA sequence, representing lung cancer, followed by its hybridization with a universal cancer biomarker anti-p53 antibody. Changes in the cyclic volatmetric and impedance signal of the graphene-gold modified electrode upon the occurrence of molecular binding events is monitored in the presence of ferri/ferro cyanide redox probe. The binding of DNA antibody has been theoretically confirmed using bioinformatic tool. Selectivity of the sensor is demonstrated using anti p21 antibody and DNA sequences from *E-Coli* pathogen. The cancer biomarker antibody can be detected in the concentration range from 0.1 ng/L to 0.1 μg/L. The minimal concentration of dsDNA required for the efficient sensing of anti-p53 antibody is 0.6 fM. Both graphene preparation and cancer biomarker sensing methods are simple, rapid, easy to fabricate, stable and can be utilized for practical applications.

1. Introduction

Simple, fast and accurate diagnosis of early cancer, a second most dangerous disease with increasing mortality rate worldwide (8.2 million per year), is utmost important for the preventive care and therapeutics. Human cancers (breast [1], liver [2], ovarian [3] and lung [4]) are the result of malfunctioning of p53 antibody, a 'guardian of the gene', that plays different activities like regulation of the cell cycle, DNA repair, and programmed cell death [5,6]. Mutated p53 gene is present in > 50% in all types of cancer cells, and identified by electro chemiluminescence, calorimetric and immuno precipitation techniques. The evolution of mutated gene increases the p53 antibody concentration in the cell and in the streaming blood and therefore, the direct estimation of serum p53 antibody as the biomarker is highly preferable over the DNA mutation screening. Binding of DNA with antibody is important to control various cellular processes such as recombination, replication, DNA repair and transcription. The dysfunction of this process induces progression of various diseases [7]. Various methods including electrophoretic mobility shift assays (EMSA) [8] or chemiluminescence assays [9], Fluorescence resonance energy transfer (FRET) techniques [10], FRET–FLIM [11], circular dichroism [12], atomic force microscopy [13], nuclear magnetic resonance [14], surface plasmon resonance [15], etc. have been employed. These methods require tedious experimental procedures and difficult to develop miniaturized portable system. These issues can be solved by employing simple, cost effective and faster electrochemical sensing method. Therefore, this work uses the double stranded DNA from lung cancer to study its binding with p53 antibody by the electrochemical method.

Graphene, a 2D material with one atom thickness available abundantly, can be used as a biosensing transducer owing to its high electronic conducting and easy biofunctionalization properties than the other similar carbon nano materials. Biofunctionalization is done either through non-covalent or by covalent attachment of biomolecule. In the non-covalent method, DNA is attached on the graphene via π-π

* Corresponding author.
E-mail address: dharumanudhay@yahoo.com (V. Dharuman).

https://doi.org/10.1016/j.sbsr.2019.100261
Received 28 November 2018; Received in revised form 22 January 2019; Accepted 25 January 2019

interaction. This method is used to pre-concentrate DNA and characterized using surface-enhanced laser desorption ionization time-of-flight mass spectrometry (SELDI-TOF-MS) [16]. For the covalent functionalization of graphene, the graphene surface is necessarily decorated or modified using either metal or other molecules containing functional groups [17,18]. Recently, *p*-aminophenol layer grafted with graphene –gold nanoparticle film electrode was reported for immunosensing [19]. The method involves electro grafting of both *p*-aminophenol and GO sequentially and decorated with gold nanoparticle for attaching the antigen. Multilayered graphene with number of layers exceeding 17 attracts high interest in the development of electronic devices along with other metals for transistor constructions [20,21] recently for the fact that the heterogeneous electron transfer rate of graphene increases regularly with number of layers [22]. The multi layered structured graphene is used energy storage, battery applications [23,24], loading of drugs, DNA, antibody and stimulated release [25–28] photo degradation of organic dye [29]. These multi layers are prepared by acid or amine functionalization of the GO. The direct adsorption of DNA or antibody on the graphene results in non-specific signal generation due to improper orientation of DNA probes indicated by fluorescence quenching method [30]. On the other hand, the label free (without using enzyme labels for signal amplification) electrochemical sensing without DNA probe degradation requires covalent linking of the capture probes. In this, a multilayerd graphene has been prepared in presence of aminoacid (glycine) by direct electrical exfoliation of pencil graphite in aqueous solution for the first time. Role of glycine in preventing graphitization is analysed using Fourier transform infrared spectroscopy, Raman, X-ray diffractommetry, X-ray photoelectron spectroscopy and transmission electron microscopy. Graphene has been decorated with gold nanoparticles prior to the biofunctionalization with DNA sequence, representing lung cancer, followed by its hybridization with a universal cancer biomarker anti-p53 antibody. Changes in the cyclic volatmetric and impedance signal of the graphene-gold modified electrode upon the occurrence of molecular binding events is monitored in the presence of ferri/ferro cyanide redox probe the dsDNA is assembled on the multilayered graphene –gold thin film via gold-thiol interactions. Sequentially, the universal cancer biomarker p53 antibody is allowed to interact with the complementary dsDNA form the dsDNA-p53 complex on the surface. The anti-p21 antibody and dsDNA from *E-coli* were used to demonstrate the selectivity of the sensor. The physicochemical and electrochemical methods are employed for the characterization of multilayerd graphene –gold composites and DNA-antibody interactions.

2. Experimental section

2.1. Materials and methods

Pencil graphite rod (0.7 mm diameter and 60 mm length) was purchased from a stationary shop. Potassium ferrocyanide, potassium ferricyanide, sodium chloride, dimethyformamide (DMF), sodium dihydrogen phosphate and potassium chloride of analytical grade were purchased from Himedia, India. Tetracholoroaurate, Anti-p53 and Anti-p21 antibodies were purchased from Invitrogen, (adjoined with fisher scientific recently). Milli-Q water (18.2 MΩ) was used for all experiments. 0.01 M phosphate buffer of pH 7.4 containing NaCl (120 mM), NaH_2PO_4 (10 mM) and KCl (2.7 mM) was prepared and used for all electrochemical experiments. 27-mer synthetic oligonucleotides representing the lung cancer DNA were synthesized by MWG biotech, Ebersberg, Germany, with HPLC purification.

Capture probe (ssDNA): 5′-HS-$(CH_2)_6$-ATC ACA GAT TTT GGG CGG GCC AAA CTG CTG-3′-II

Complementary target(dsDNA): 5′-CAG CAG TTT GGC CCG CCC AAA ATC TGT GAT-3′-II

E-coli DNA sequences

Capture probe (ssDNA): 5′-HS-$(CH_2)_6$-CGA TCT GTT TTA TGT AGG GTT AGG TCA-3′ -III

Complementary target (dsDNA): 5′-TGA CCT AAC CCT ACA TAA AAC AGA TCG-3′ -IV

All DNA samples were prepared in SSC buffer (saline-sodium citrate buffer, pH 7.0). pH meter from Susima, AP-1PLVS, India, was used for measuring the solution pH. A conventional three electrode cell consisting of Ag/AgCl reference electrode, Pt wire counter electrode and 2 mm diameter Au disk working electrode having 0.03 cm^2 geometric areas was used for all electrochemical measurements. The Au electrode was initially treated with piranha solution for 30 min, and rinsed thoroughly with distilled water. The electrode was then polished using Al_2O_3 powder (5.0, 1.0 and 0.05 mM), and sonicated in Milli Q water. CV and EIS were performed using a 6500D electrochemical analyzer from CH Instruments, Texas, USA, in presence of 1 mM $[Fe(CN)_6]^{3-/4-}$ in PBS buffer (pH 7.4). The CV was recorded in the potential window −200 to +600 mV at a scan rate 50 mV s^{-1}. The EIS measurements were made by applying an ac potential amplitude ± 5 mV over the dc potential 250 mV (redox potential of 1 mM $[Fe(CN)_6]^{3-/4-}$ at gold electrode in PBS) in the frequency range 100 kHz – 1 Hz. Impedance data were plotted in the form of Nyquist plot. Zsimpwin software was used to determine the charge transfer resistance (R_{CT}). The EIS profile is matched with Randles equivalent circuit [R_s ($Q_{CPE}R_{CT}$)W] with chi square value 5.005×10^{-4}. In this circuit, Rs is the background solution resistance, R_{CT} the charge-transfer resistance, Q_{CPE} the electrical double layer capacitance and W the Warburg coefficient.

PANalytical make Bruker D8-Advance powder diffractometer which uses Cu-Kα1 radiation (2.2 kW max) was used for powder X-ray diffraction measurements (PANalytical B.V., Lelyweg 1, 7602 EA ALMELO, The Netherlands). Chemical Vapour Deposited gold (100 nm), Si and graphite substrates were used for acquiring the FE-SEM images and EDS spectra from Zeiss SEM instrument Hitachi (model S−3000H), Japan which uses a LEO 1530 field emission. Images were recorded at an accelerating voltage 10 kV with a secondary electron detector.

2.2. Simultaneous electrical exfoliation and reduction of pencil graphite by glycine

Homemade variable DC power supply with Digital multimeter was used for applying a constant DC potential +7 V between two pencil electrodes in presence of 0.1 M glycine. Thus obtained graphene was washed with double distilled water, ethanol, acetone and filtration by centrifuging at 8000 rpm for 5 min. The final product was dried at 45 °C for 2 h, Scheme 1 and named as g-G. The graphene product was confirmed by both electrochemical and physicochemical characterization techniques (XRD, Raman, XPS, FTIR, TEM and FESEM).

2.3. Electrode modification

For modifying the gold electrode (AuE) surface with the above synthesized g-G, 1.5 mg of g-G was dispersed in 1 mL DMF followed by sonication for 15 min. 2 μL of the mixture was drop casted on the AuE and dried at an ambient temperature for 1 h. For the immobilization of ssDNA on the g-G, the graphene modified AuE surface was further decorated with AuNP prepared by citrate reduction method [31]. 2 μL of 1 μM thiolated ssDNA probe was dropped onto the modified electrodes and incubated for 1 h under humid conditions and washed with the blank PBS buffer to remove the un-reacted ssDNAs [32]. 2 μL of 1 μM target DNA (target II Section 2.1) was drop casted on the g-G-AuNP-ssDNA modified electrode to hybridize with the ssDNA to form complementary dsDNA for 1 h under identical experimental conditions. The electrochemical studies were carried out by CV and EIS techniques intermittently in the PBS pH 7.4 in the presence of 1 mM $[Fe(CN)_6]^{3-/4-}$. Antibody interaction with the preformed dsDNA was made by incubating the dsDNA modified surface with 2 μL of 0.1 μg/L anti-p53 antibody for 1 h under identical experimental conditions. Same protocol was followed for the negative control experiment using the *E-coli* dsDNA and anti-p21 antibody in the selectivity experiments.

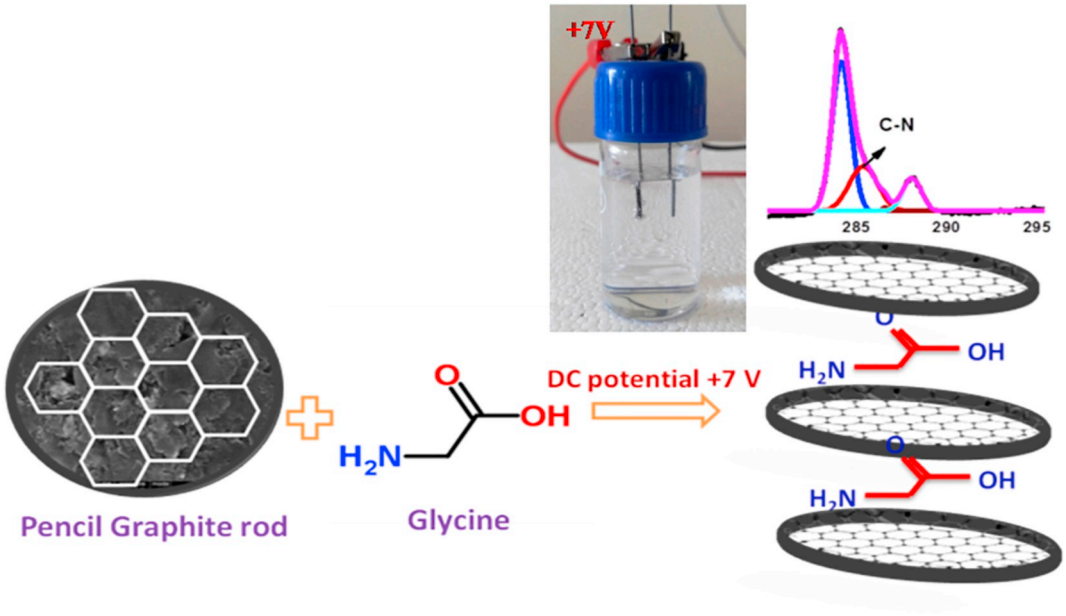

Scheme 1. Direct electrical exfoliation of pencil graphite in presence of glycine.

2.4. Antibody preparation, DNA modelling and molecular docking of selective DNA fragment and anti-p53 antibody

Three dimensional DNA model was generated using the DNA Analysis and Rebuilding program (3D-DART) [33]. 3D-DART online server modeled the DNA structure in canonical B-DNA conformation with reference to the available DNA structures and the overhanging base-pairs were converted to all-paired structures in accordance to Watson–Crick counterparts. The crystal structure of Anti-p53 antibody bound with Zinc metal was retrieved from Antibody Data Bank [PDB ID: 2i00] [34]. Further, the antibody was optimized and minimized in Schrodinger Antibody preparation wizard [35]. HDOCK server is a hybrid docking algorithm, which implies a FFT-based global docking protocol to sample the binding modes [36]. Antibody-DNA docking was performed with default parameters to explore the binding properties of the target DNA in the P53 antibody.

3. Results and discussion

3.1. Electrochemical characterization of glycine functionalized multi layer graphene

Electrochemical properties of the graphite, graphene oxide (GO) and g-G are examined by cyclic voltammetry in the presence of $[Fe(CN)_6]^{3-/4-}$ redox probe in PBS (pH 7.4), Fig. 1. Both the graphite and g-G show higher peak currents (example i_{pa} 9.71 and 11.7 μA ΔE_p*(peak-to-peak separation)* 110 and 90 mV, respectively), compared to the GO modified AuE that shows lower peak current (i_{pa}: 4.4 μA) with increased peak-to-peak separation ΔE (ΔE_p: 160 mV). Among the graphite and g-G modified surfaces, higher reversible redox behavior was observed for the g-G (Curve e, g., anodic peak current i_{pa} 11.7 μA) with lower ΔE_p (90 mV). This is related to the formation of thin layered graphene by the in-situ exfoliation and reduction processes. In order to confirm the presence of functional groups on the g-G, the g-G modified gold electrode was potential cycled in the pure PBS solution and observed a diffused reduction peak (at −1.0 V) (Fig. S1A). This reduction peak is completely disappeared in the second cycle itself. This behavior is quite similar to the electrochemical reduction of GO [37–39] indicating the presence of few carboxyl functional groups on the g-G. After this experiment, the g-G modified surface is reinvestigated for its charge transport properties in the presence of $[Fe(CN)_6]^{3-/4-}$ and observed no

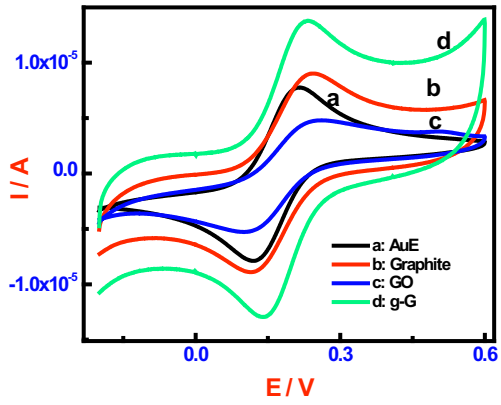

Fig. 1. CV behaviors of unmodified (curve a), graphite (curve b), GO (cure c) and g-G (curve d) modified Au electrode measured in presence of $[Fe(CN)_6]^{3-/4-}$ in PBS (pH 7.4) at a scan rate 50 mVs^{-1}.

signature of charge transport^{-}, but exhibits a large charging current than the unreduced g-G, Fig. S1B. This is again contradictory with the observations made electrochemically for the reduced GO [37–39] which exhibits higher charge transfer property than the unreduced GO. Therefore, these behaviors indicate that when a strong reduction potential was applied on the g-G modified surface, the intercalated glycine may undergo self polymerization to form non-conducting film, preventing the heterogeneous electron transfer from the $[Fe(CN)_6]^{3-/4-}$ (Fig.S1B). That is, glycine is attached on the graphene during the electrical exfoliation of graphene. Because the GO surface stabilized glycine reduces the charge transport, its reduction is prevented by applying the potential window between −200 to 700 mV (Ag/AgCl) for further studies. The role of glycine in the formation of graphene is further examined by the physicochemical characterization of the g-G.

The XRD and Raman behaviors of the graphite, GO and g-G are presented comparatively in Fig. 2. From the XRD pattern in Fig. 2A, it is noted that the graphite exhibits peaks at 2θ 26.5° and 54.5° corresponding to the (002) and (004) planes, respectively, while the g-G showed only the (002) plane at 2θ 25.8° with broad and low intensity. This is attributed to the random packing of graphene sheets which arises from the reduced structural defects in the g-G [40,41]. In the Raman spectroscopy, Fig. 2B, the graphite exhibits G-band (at

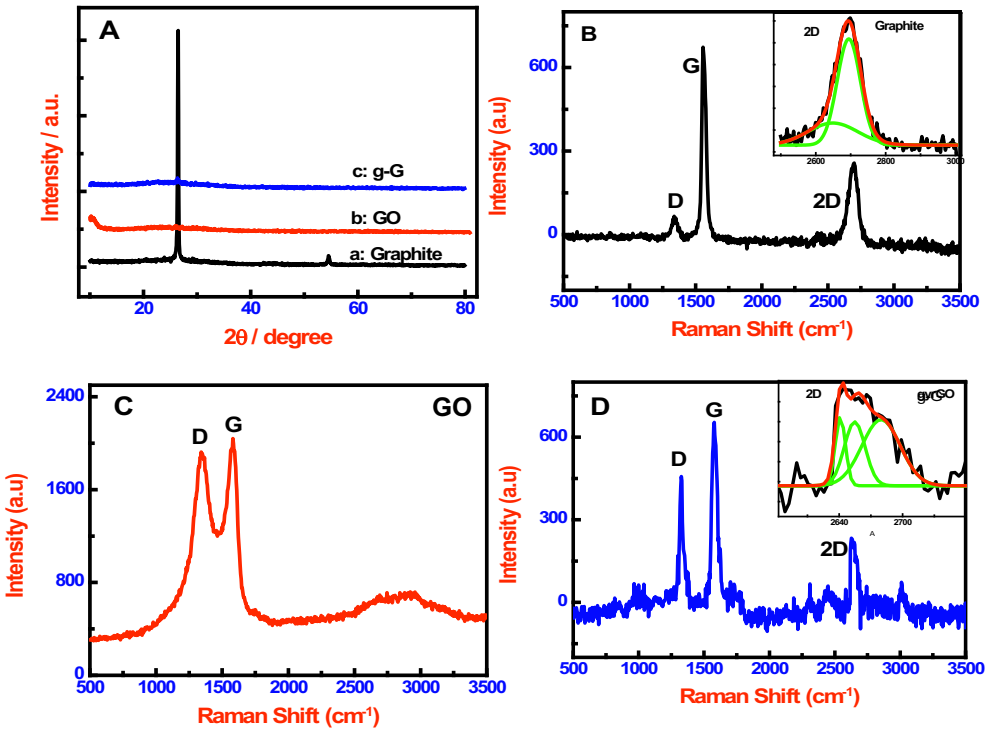

Fig. 2. (A) XRD pattern and (B) Raman spectra of graphite (curve a), GO (curve b) and g-G (curve c).

1562 cm^{-1}) and a sharp 2D-band (at 2699 cm^{-1}) corresponding to the first order scattering of the E_{2g} vibration mode and the second-order two phonon mode, respectively. Moreover, a weak D-band, arising from the disorder induced mode due to the presence of less structural defects, is also observed for the graphite at 1342 cm^{-1}. The intensity ratio of D and G bands (I_D/I_G) is a measure of the presence of disorders and is inversely proportional to the average size of the sp^2 clusters [42]. For the graphite, the observed I_D/I_G ratio was 0.07 nm. The D band for the g-G located at 1344 cm^{-1} is resulted from the defect-induced breathing mode of sp^2 rings [43]. The G band at 1598 cm^{-1} for the g-G is due to the first order scattering of the E_{2g} phonon of sp^2 carbon atoms. The intensity of the D band is related to the size of the in-plane sp^2 domains [44] and its increased intensity indicates the formation of more sp^2 domains. Higher I_D/I_G ratio for the g-G (0.6) than the graphite (0.07) signatures the presence of higher amount of structural defects induced by the introduction of oxygen functional groups during the simultaneous exfoliation and reduction processes in presence of glycine. This is confirmed by the electro reduction of functional groups present in g-G, Fig. S1A. Further, the increased I_{2D}/I_G ratio 0.4 obtained for the g-G compared to the graphite (I_{2D}/I_G: 0.38) indicates the presence of defects and the intercalated glycine in the g-G layer and prevention of graphitization by the restacking of the exfoliated GO. Hence, the g-G showed enhanced CV peak currents compared to the graphite in the presence of $[Fe(CN)_6]^{3-/4-}$.

Coordination of glycine with the g-G is further confirmed from the FTIR (Fig. S2) and XPS (Fig. 3A and B) spectral behaviors. Intensities of FTIR bands in the frequency region 1000 to 1800 cm^{-1} are decreased effectively for both the graphite and g-G compared to the unreduced GO which consists of alkoxy C—O stretching vibrations (1086 cm^{-1}), aromatic C = C (1620 cm^{-1}) stretching and O—H stretching (3450 cm^{-1}). The presence of weak intense peaks at 1330 and 1550 cm^{-1} in the FTIR spectra of g-G indicate the C—N and C—H bending arising from the intercalated glycine [45]. Similarly, the C1s spectrum of g-G (Fig. 3B) showed higher intensity C=C band (284.5 eV), lower intensity C=O band (288.4 eV) with a new C—N band at 285.4 eV compared to the unreduced GO (Fig. 3A), indicating the restoration of pi-electron network due to the reductive interaction nature of the glycine [45] with the g-G, Scheme 1.

The TEM (Fig. 3C and D) and HRSEM (Fig. S3) show flake like structure for the GO, whereas a thin layered film structure for the g-G, Fig. 3. The interlayer distance 0.38 nm obtained from the TEM along with XRD peak broadening and higher I_{2D}/I_G (0.4) [40] again confirms the presence of glycine in the thin layer g-G.

3.2. DNA functionalized g-G for label free selective sensing of anti-p53 antibody

For the orientation controlled immobilization of DNA on the g-G, the AuNPs were used to decorate the g-G by electrostatic interaction [46]. Following this, the thiolated single stranded DNA (HS-ssDNA) was immobilized through gold–thiol chemistry on the g-G-AuNP. Fig. 4A shows that the immobilizations of HS–ssDNA on the g-G-AuNP lowered the peak currents (Table S1, 7.37 μA) and increased ΔEp (200 mV, peak-to-peak separation) and R_{CT} values (Fig. 4B and Table S2, 1.713 × 104 Ω cm^{-2}) compared to the g-G-AuNP modified electrode (10.6 μA, 100 mV and 8.08 × 103 Ω cm^{-2}). This is due to the electro static repulsion between the negatively charged immobilized ssDNA and $[Fe(CN)_6]^{3-/4-}$. Further, hybridization with the complimentary ssDNA (target II) to form a perfect double stranded DNA (dsDNA) increased further the R_{CT} (4.999 × 10^4 Ω cm^{-2}), ΔEp (230 mV) and decreases the peak current (5.35 μA) compared to the ssDNA surface, attributed to the increased negative charges and molecular layer thickness. These observations are in agreement with the previous literature reports [17,18]. In contrast, hybridization with the complete non-complementary target DNA showed insignificant change in the CV and EIS profiles compared to the ssDNA immobilized surface. These data indicate the efficient discrimination of the complementary and non-complementary hybridization by the multi layered g-G–AuNP composite film sensor. The complementary dsDNA formed surface is utilized further for the anti-p53 antibody binding.

P53 is a universal cancer biomarker and p53 antibody interaction with DNA is reported for the early diagnosis of cancer using immono

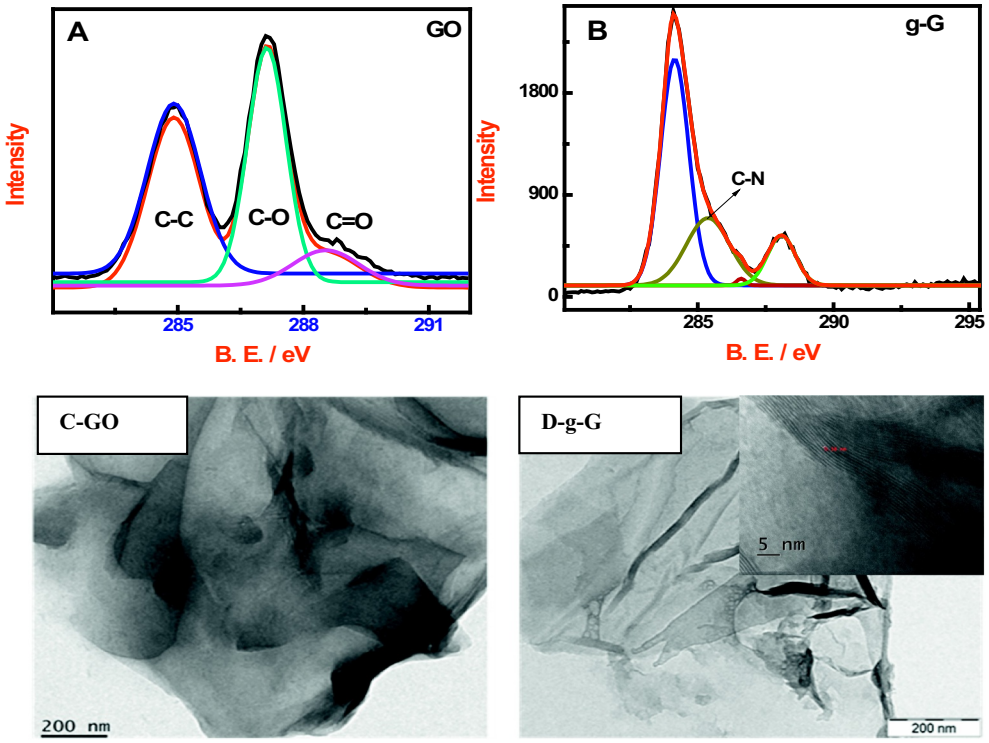

Fig. 3. C1s XPS spectra of GO (A) and g-G (B). TEM image of GO (C) and g-G (D).

sensing principle [47]. Two different electrodes having dsDNA with identical electrochemical behaviors were prepared. On each surface, both the tumor suppressor anti-p53 and non tumor suppressor anti p21 (control antibody) antibodies were allowed to interact for 1 h and washed with blank PBS to remove the unreacted antibodies on the surface. CV and EIS behaviors of these surfaces are depicted in Fig. 5A&B, Scheme 2.

The interaction of target anti-p53 antibody results in decreased CV peak currents (Table S3, i_{pa}: from 5.35 μA to 3.53 μA), increased ΔEp (from 230 mV to 240 mV) and R_{CT} (Fig. S4A and Table S4, 4.99×10^4 to $9.88 \times 10^4\ \Omega\,cm^{-2}$). The interaction of control anti-p21 antibody shows insignificant change in the CV and EIS profiles (Table S3, from 5.35 μA to 5.36 μA). Interaction of either anti-p53 and anti p21 antibodies with the ssDNA modified showed insignificant change in the electronic signal indicating no complex of DNA-antibody complex formation. A similar experiment made by the interactions of anti-p53 and anti-p21 antibodies with the pathogenic *E-Coli* complementary dsDNA modified electrode exhibits negligible changes in the CV (Fig. 5B, Scheme 2) and EIS profiles (Fig. S4B). Hence, the anti-p53 antibody selectively binds only with the lung cancer complementary dsDNA and not with the *E-Coli* complementary DNA. This confirms the fact that the sensor can discriminate the cancer and pathogenic affected samples. To validate this binding of lung cancer dsDNA with the p53 antibody, an *in-silico* experiment has been conducted using bioinformatic tools.

Further the DNA-antibody interaction has been studied by computational Rebuilding program (3D-DART) [33]. 3D single stranded structure of target lung cancer DNA (30 bases) was modeled in 3D-DART tool. The Anti-p53 antibody complexed with Zinc metal was retrieved from Antibody Data Bank (PDB) is prepared in Schrodinger suite to assign proper bond orders, lengths and addition of hydrogen atoms. Refined antibody structure was used as the semi-flexible input for docking analysis. Since the study is intended to find the binding properties of target DNA, HDOCK server automatically predicts the favorable binding sites in the antibody and docks the target DNA provided in 3D conformation onto the predicted binding site. The docking protocol of HDOCK scanned the favorable regions of anti-p53 receptor and bound the modeled DNA by docking algorithm. The anti- p53 antibody - DNA complex shown the HDOCK score of −537.96, high

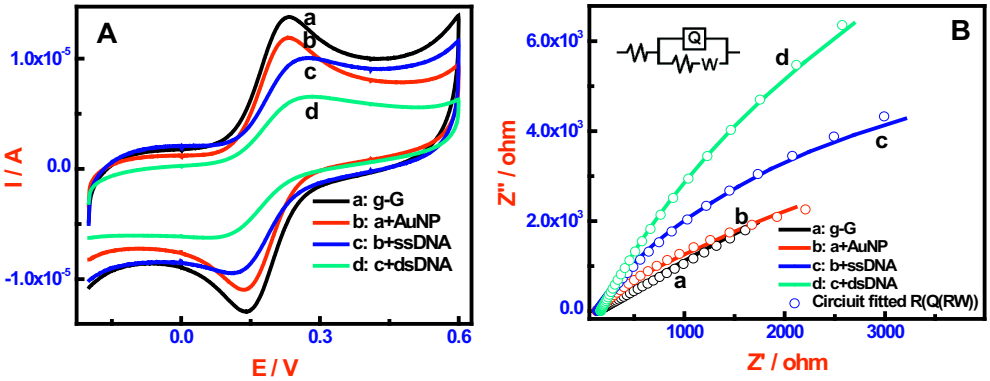

Fig. 4. (A) Cyclic voltammetery and (B) EIS behaviors of g-G-AuNP modified electrodes with sequential addition of AuNP (b), ssDNA (c), dsDNA (d), recorded in phosphate buffer (pH 7.4) in presence of 1 mM $[Fe(CN)_6]^{3-/4-}$. Star line: (R(RQ)W) equivalent circuit fit data.

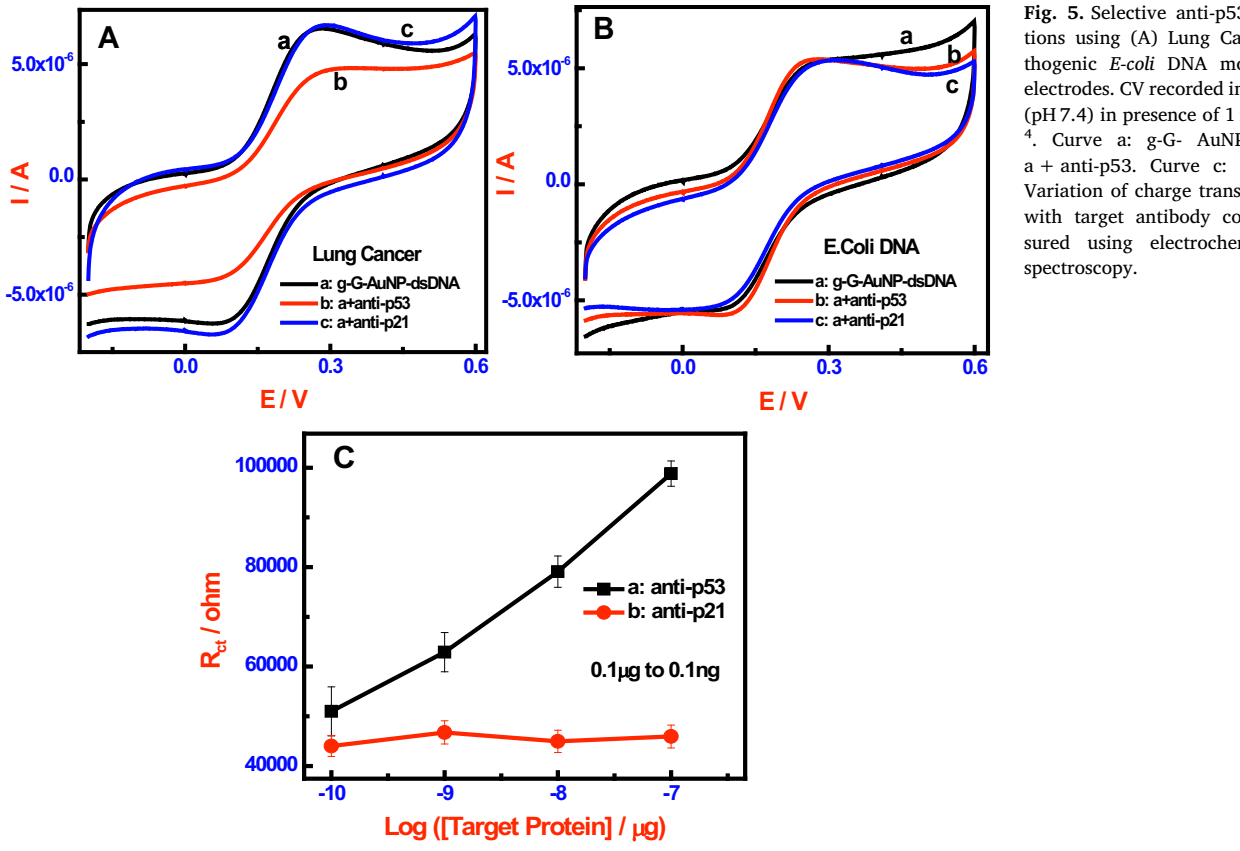

Fig. 5. Selective anti-p53 antibody detections using (A) Lung Cancer and (B) pathogenic *E-coli* DNA modified g-G-AuNP electrodes. CV recorded in phosphate buffer (pH 7.4) in presence of 1 mM $[Fe(CN)_6]^{3-/4}$. Curve a: g-G- AuNP-DNA. Curve b: a + anti-p53. Curve c: a + anti-p21. (C) Variation of charge transfer resistance R_{CT} with target antibody concentration measured using electrochemical impedance spectroscopy.

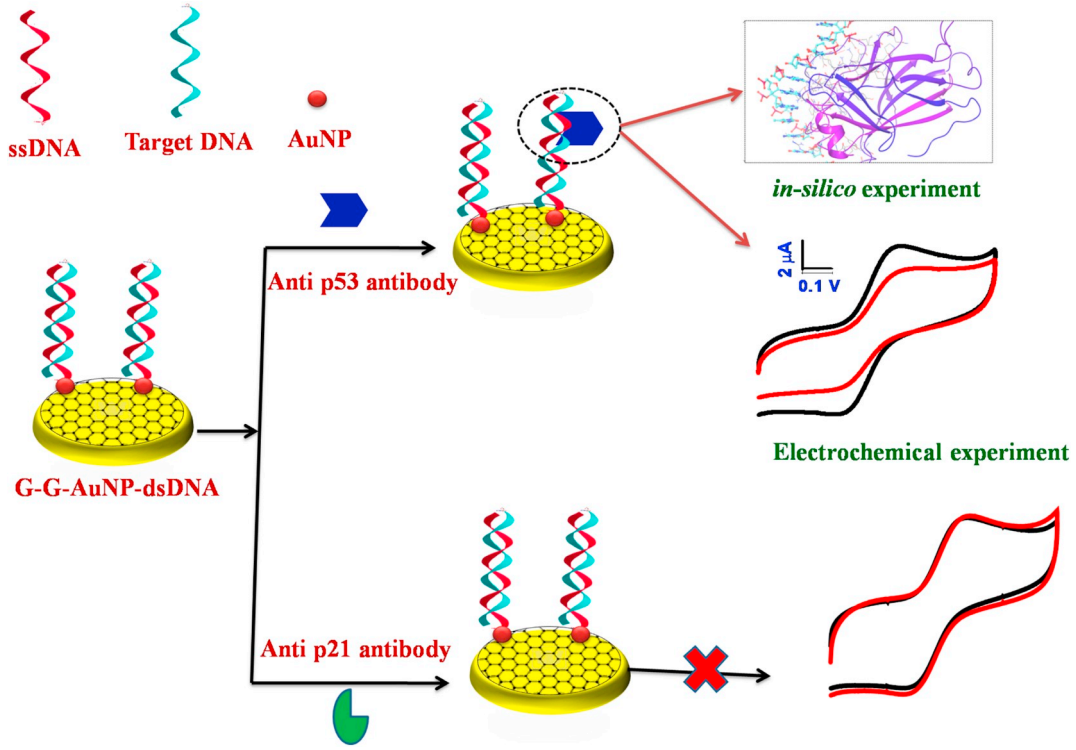

Scheme 2. Selective label free DNA-anti-p53 antibody sensing at g-G-AuNP sensor surface by electrochemical method.

negative values indicates the higher binding affinity of the target DNA with the anti-p53 antibody (Fig. 6). The antibody - DNA complex is stabilized by the two hydrogen bonds (Lys1232……Cyt18 and Lys1136……Ade19) and supported by aromatic interaction (His1165……Thy27). Apart from these three interactions, several positive contacts were observed between the surface of receptor and legend DNA molecule. Lys1232 and Lys1136 residue has formed hydrogen bonds with Adenine18 and 19 at the distance of 2.56 and 2.68

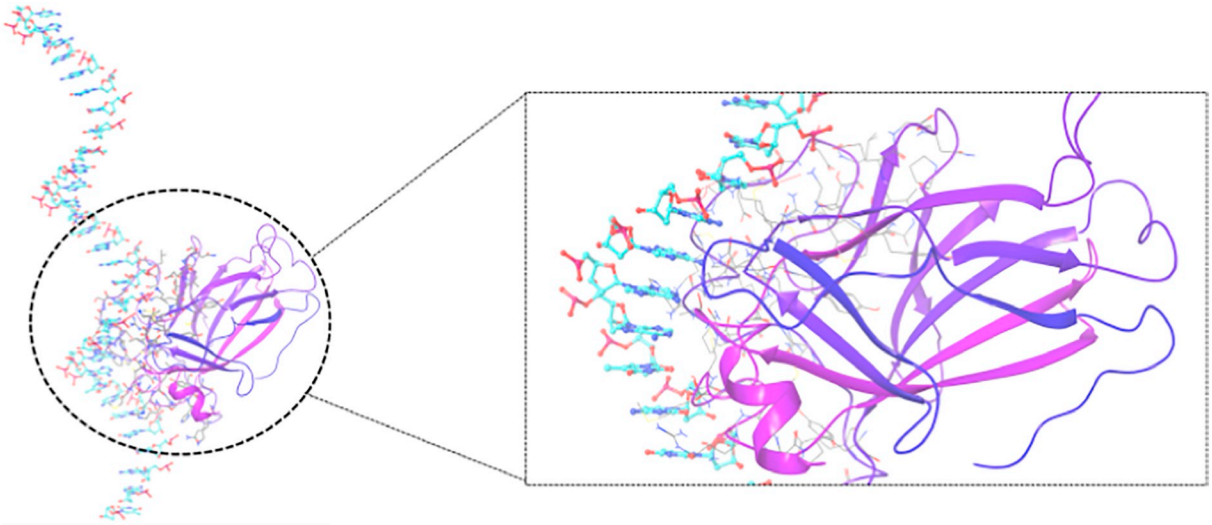

Fig. 6. Interaction insights of DNA in Anti-p53 antibody. The hydrogen bonds formed between Lys1232……Cyt18 and Lys1136……Ade19 were represented by red dotted lines. (For interpretation of the references to colour in this figure legend, the reader is referred to the web version of this article.)

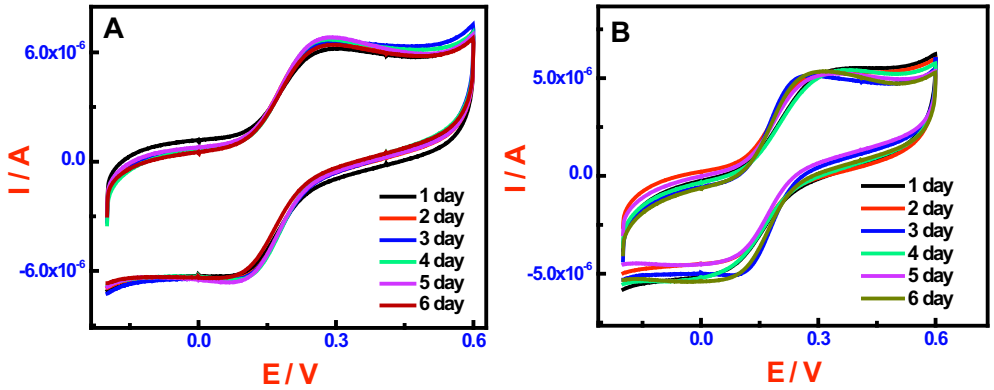

Fig. 7. Study of stability of g-G-AuNP-dsDNA (A) and g-G-AuNP-dsDNA-p53 (B) modified electrodes monitored voltammetrically in presence of 1 mM $[Fe(CN)_6]^{3-/4-}$ in phosphate buffer.

respectively. Similarly the aromatic bond was observed between the His1165 residue and Thymine27 at a distance of 2.37. Based on the interaction, it is evident that the lung cancer DNA is interacting to anti-p53 antibody with high affinity and the structural level interactions observed were confirming the experimental results. This experiment proves the highly selective sequence specific interaction nature of the sensor in detecting the p53 cancer biomarker. The concentration studies were made on g-G-AuNP-dsDNA modified electrode and the linear range obtained was 0.1 ng/L to 0.1 μg/L (Fig. 5C). The observed lowest detection limit of p53 antibody biomarker is almost comparable with the literature report ($0.1 pgmL^{-1}$ = 0.1 ng/L) on the graphene-AuNP composite using immunochemistry [19]. However, we have not used the self assembled monolayer for anchoring GO and its subsequent reduction by electrochemical method.

Reproducibility data presented in Fig. S5 are for the four repeated measurements obtained using four different DNA-anti p53 modified surfaces prepared under similar experimental conditions. The closeness of the data reveals the high reproducibility nature of the sensor developed. The stability of G-G-AuNP-dsDNA and G-G-AuNP-dsDNA-anti p53 antibody layers are modified on two different AuEs are validated for the stability for on six days and presented in Fig. 7. The electrodes show very small and negligible change in the anodic peak currents for all surfaces examined, indicating the excellent ultra sensitivity, selectivity, stability, and reproducibility of sensor in both the studies of DNA and DNA-anti p53 antibody binding. The lowest concentration of dsDNA required for the efficient signal generation using this newly prepared graphene-AuNP composite has been evaluated by the studying the concentration of dsDNA formation on the surface and signal generation in presence of anti p53 antibody. It is noted that the concentration of 0.6 fM of dsDNA is enough to observe the change in the electrochemical signal.

4. Conclusion

Direct electrical exfoliation of graphene in presence of glycine results in the formation of few layered graphene indicated by the appearance of high intense G and D bands with the I_{2D}/I_G ratio 0.4. The FTIR and XPS data indicates the presence of CN bonding from the glycine in the graphene. This may be due to the interaction of amphiphile glycine by the electrostatic interaction with the oxy functional groups, supported by the observation of poor charge transfer in the presence of $[Fe(CN)_6]^{3-/4-}$ due to the formation of poly glycine. Detection of selective label free binding of lung cancer dsDNA with anti p53 antibody biomarker was achieved by electrochemical method on the graphene-gold nanoparticle composite thin film in the concentration range 0.1 ng/L–0.1 μg/L. This platform could be easily prepared and implemented in different applications.

Acknowledgement

The authors H. Imran and V. Dharuman gratefully acknowledge the financial support of University Grants Commission, Major Research Project Ref: F. No.43-304/2014(SR) dated 3.09.2015, New Delhi, India and RUSA 2.0 [F.24-51/2014-U, Policy (TN Multi-Gen), Dept of Edn, Gol]. P. N. Manikandan acknowledges the Department of Science and Technology of India for the award of INSPIRE Fellowship (IF 140744). J. H. Hahn thanks the financial support from the Basic Science Research Program through the National Research Foundation of Korea (NRF) funded by the Ministry of Education (NRF-2018R1D1A1B07046959).

Appendix A. Supplementary data

Supplementary data to this article can be found online at https://doi.org/10.1016/j.sbsr.2019.100261.

References

[1] S. Metcalfe, T.K. Wheeler, S. Picken, S. Negus, A.J. Milner, P53 autoantibodies in 1006 patients followed up for breast cancer, Breast Cancer Res. 2 (2000) 438–443.
[2] M.M. Atta, S.A. El-Masry, M. Abdel-Hameed, H.A. Baiomy, N.E. Ramadan, Value of serum anti-p53 antibodies as a prognostic factor in Egyptian patients with hepatocellular carcinoma, Clin. Biochem. 41 (2008) 1131–1139.
[3] K.S. Anderson, J. Wong, A. Vitonis, P. Crum, P.M. Sluss, J. LaBaer, D. Cramer, p53 autoantibodies as potential detection and prognostic biomarkers in serous ovarian cancer, Cancer Epidemiol. Biomark. Prev. 19 (2010) 859–868.
[4] M. Cioffi, M.T. Vietri, P. Gazzerro, R. Magnetta, A. D'Auria, A. Durante, E. Nola, G.A. Puca, A.M. Molinari, Serum anti-p53 antibodies in lung cancer: comparison with established tumor markers, Lung Cancer 33 (2001) 163–169.
[5] B. Vogelstein, D. Lane, A.J. Levine, Surfing the p53 network, Nature 408 (2000) 307–310.
[6] D.P. Lane, Cancer p53, guardian of the genome, Nature 358 (1992) 15–16.
[7] A.B. Williams, B. Schumacher, p53 in the DNA-damage-repair process, Cold Spring Harb. Perspect. Med. 6 (2016) 026070.
[8] L.M. Hellman, M.G. Fried, Electrophoretic mobility shift assay (EMSA) for detecting protein-nucleic acid interactions, Nat. Protoc. 2 (2007) 1849–1861.
[9] N. Bhattacharya, A. Sarno, I.S. Idler, et al., High-throughput detection of nuclear factor- kappaB activity using a sensitive oligo-based chemiluminescent enzyme-linked immunosorbent assay, Int. J. Cancer 127 (2010) 404–411.
[10] A.I. Dragan, P.L. Privalov, Use of fluorescence resonance energy transfer (FRET) in studying protein-induced DNA bending, Methods Enzymol. 450 (2008) 185–199.
[11] F.G. Cremazy, E.M. Manders, P.I. Bastiaens, G. Kramer, G.L. Hager, E.B. Munster, P.J. Verschure, TJ.Jr. Gadella, R. Driel, Imaging in situ protein-DNA interactions in the cell nucleus using FRET-FLIM, Exp. Cell Res. 309 (2005) 390–396.
[12] P.D. Cary, G.G. Kneale, Circular dichroism for the analysis of protein-DNA interactions, Methods Mol. Biol. 543 (2009) 613–624.
[13] Y.L. Lyubchenko, A.A. Gall, L.S. Shlyakhtenko, Visualization of DNA and protein-DNA complexes with atomic force microscopy, Methods Mol. Biol. 1117 (2014) 367–384.
[14] S. Campagne, V. Gervais, A. Milon, Nuclear magnetic resonance analysis of protein–DNA interactions, J. R. Soc. Interface 8 (2011) 1065–1078.
[15] P.G. Stockley, B. Persson, Surface plasmon resonance assays of DNA-protein interactions, Methods Mol. Biol. 543 (2009) 653–669.
[16] H.M. Rawel, S. Rohn, J. Kroll, F.J. Schweigert, Surface enhanced laser desorptions ionization-time of flight-mass spectrometry analysis in complex food and biological systems, Mol. Nutr. Food Res. 49 (2005) 1104–1111.
[17] H. Imran, P.N. Manikandan, V. Dharuman, Graphene oxide supported liposomes for efficient label freeelectrochemical DNA biosensing, Sensors Actuators B 260 (2018) 841–851.
[18] K. Jayakumar, B.C. Maria, V. Dharuman, J. Huangxian, S.D. Ramendra, W. Yangping, One-step coelectrodeposition-assisted layer-by-layer assembly of gold nanoparticles and reduced graphene oxide and its self-healing three-dimensional nanohybrid for an ultrasensitive DNA sensor, Nanoscale 10 (2018) 1196–1206.
[19] R. Elshafey, M. Siaj, A.C. Tavares, Au nanoparticle decorated graphene nanosheets for electrochemical immunosensing of p53 antibodies for cancer prognosis, Analyst 141 (2016) 2733–2740.
[20] H.-L. Tang, M.-H. Chiu, C.-C. Tseng, S.-H. Yang, K.-J. Hou, S.-Y. Wei, J.-K. Huang, Y.-F. Lin, C.-H. Lien, L.-J. Li, Multilayer graphene–WSe2 heterostructures for WSe2 transistors, ACS Nano 11 (2017) 12817–12823.
[21] Y. Henni, H. Collado, K. Nogajewski, M.R. Molas, G. Usaj, C.A. Balseiro, M. Orlita, M. Potemski, C. Faugeras, Rhombohedral multilayer graphene: a magneto-Raman scattering study, Nano Lett. 16 (2016) 3710–3716.
[22] A.G. Guell, N. Ebejer, M.E. Snowden, J.V. Macpherson, P.R. Unwin, Electrochemistry at single-walled carbon nanotubes: the role of band structure and quantum capacitance, J. Am. Chem. Soc. 134 (2012) 7258–7261.
[23] E. Greco, G. Nava, R. Fathi, F. Fumagalli, A.E.D. Rio-Castillo, A. Ansaldo, S. Monaco, F. Bonaccorso, V. Pellegrini, F.D. Fonzo, Few-layer graphene improves silicon performance in Li-ion battery anodes, J. Mater. Chem. A 5 (2017) 19306–19315.
[24] D-S. Kim, H. Kwon, A.Y. Nikitin, S. Ahn, L. Martín-Moreno, García-Vidal, F.J. Sunmin Ryu, H. Min, Z.H. Kim, Stacking structures of few-layer graphene revealed by phase- sensitive infrared Nanoscopy, ACS Nano, 9 (2015) 9 6765–6773.
[25] A.J. Khopade, F. Caruso, Electrostatically assembled polyelectrolyte/dendrimer multilayer films as ultrathin nanoreservoirs, Nano Lett. 2 (2002) 415–418.
[26] T. Crouzier, K. Ren, C. Nicolas, C. Roy, C. Picart, Layer-by-layer films as a biomimetic reservoir for rhBMP-2 delivery: controlled differentiation of myoblasts to osteoblasts, Small 5 (2009) 598–608.
[27] C.J. Ochs, G.K. Such, Y. Yan, M.P. Koeverden, F. Caruso, Biodegradable click capsules with engineered drug-loaded multilayers, ACS Nano 4 (2010) 1653–1663.
[28] K.I. MacConaghy, D.M. Chadly, M.P. Stoykovich, J.L. Kaar, Label-free detection of missense mutations and methylation differences in the p53 gene using optically diffracting hydrogels, Analyst 140 (2015) 6354–6362.
[29] S. Umrao, P. Sharma, A. Bansal, R. Sinha, R.K. Singh, A. Srivastava, Multi-layered graphene quantum dots derived photodegradation mechanism of methylene blue, RSC Adv. 5 (2015) 51790–51798.
[30] B. Liu, S. Salgado, V. Maheshwari, J. Liu, Bioresponsive DNA-co-polymer hydrogels for fabrication of sensors, Curr. Opin. Colloid Interface Sci. 26 (2016) 1–9.
[31] G. Frens, Controlled nucleation for the regulation of the particle size in monodisperse gold suspensions, Nat. Phys. Sci. 241 (1973) 20–22.
[32] V. Dharuman, K. Vijayaraj, S. Radhakrishnan, T. Dinakaran, J. Shankara Narayanan, M. Bhuvana, J. Wilson, Sensitive label-free electrochemical DNA hybridization detection in the presence of 11-mercaptoundecanoic acid on the thiolated single strand DNA and mercaptohexanol binary mixed monolayer surface, Electrochim. Acta 56 (2011) 8147–8155.
[33] M. van Dijk, A.M.J.J. Bonvin, 3D-DART: a DNA structure modelling server, Nucl. Acids Res. 37 (2009) 235–239.
[34] H.M. Berman, J. Westbrook, Z. Feng, G. Gilliland, T.N. Bhat, H. Weissig, I.N. Shindyalov, P.E. Bourne, The protein data bank, Nucl. Acids Res. 28 (2000) 235–242.
[35] D. Prabhu, R. Vidhyavathi, J. Jeyakanthan, D. Prabhu, R. Vidhyavathi, J. Jeyakanthan, Computational identification of potent inhibitors for streptomycin 3″-adenylyltransferase of Serratia marcescens, Microb. Pathog. 103 (2017) 94–106.
[36] Y. Yan, D. Zhang, P. Zhou, B. Li, S.-Y. Huang, S.-Y. Huang, HDOCK: a web server for protein–protein and protein–DNA/RNA docking based on a hybrid strategy, Nucl. Acids Res. 45 (2017) 365–373.
[37] J. Kauppila, P. Kunnas, P. Damlin, A. Viinikanoja, C. Kvarnstrom, Electrochemical reduction of graphene oxide films in aqueous and organic solutions, Electrochim. Acta 89 (2013) 84–89.
[38] S.Y. Toh, K.S. Loh, S.K. Kamarudin, W.R.W. Daud, Graphene production via electrochemical reduction of graphene oxide: synthesis and characterization, Chem. Eng. J. 251 (2014) 422–434.
[39] H. Imran, P.N. Manikandan, V. Dharuman, Facile and green synthesis of graphene oxide by electrical exfoliation of pencil graphite and gold nanoparticle for non-enzymatic simultaneous sensing of ascorbic acid, dopamine and uric acid, RSC Adv. 5 (2015) 63513–63520.
[40] H. Tang, P. Gao, X. Liu, H. Zhua, Z. Bao, Bio-derived calcite as a sustainable source for graphene as high-performance electrode material for energy storage, J. Mater. Chem. A 2 (2014) 15734–15739.
[41] A. Chakrabarti, J. Lu, J.C. Skrabutenas, T. Xu, Z.L. Xiao, J.A. Maguire, N.S. Hosmane, Conversion of carbon dioxide to few-layer graphene, J. Mater. Chem. 21 (2011) 9491.
[42] M.A. Pimenta, G. Dresselhaus, M.S. Dresselhaus, L.G. Cancado, A. Jorio, R. Saito, Studying disorder in graphite-based systems by Raman spectroscopy, Phys. Chem. Chem. Phys. 9 (2007) 1276.
[43] A. Kaniyoor, S. Ramaprabhu, A Raman spectroscopic investigation of graphite oxide derived graphene, AIP Adv. 2 (2012) 032183.
[44] K.N. Kudin, B. Ozbas, H.C. Schniepp, R.K. Prudhomme, I.A. Aksay, R. Car, Raman spectra of graphite oxide and functionalized graphene sheets, Nano Lett. 8 (2008) 36.
[45] S. Bose, T. Kuila, A.K. Mishra, N.H. Kim, J.H. Lee, Dual role of glycine as a chemical functionalizer and a reducing agent in the preparation of graphene: an environmentally friendly method, J. Mater. Chem. 22 (2012) 9696–9703.
[46] K. Turcheniuk, R. Boukherroub, S. Szunerits, Gold–graphene nanocomposites for sensing and biomedical applications, J. Mater. Chem. B 3 (2015) 4301–4324.
[47] Y. Zhou, Z. Wang, W. Yue, K. Tang, W. Ruan, Q. Zhang, L. Liu, Label-free detection of p53 protein using a microcantilever biosensor with piezoresistive readout, IEEE Sens. Conf. (2009) 819–822.